International Journal for Housing Science and Its Applications
Publish August 10, 2025. Volume 46, Issue 4 Pages 8351-8369

https://doi.org/10.70517/ijhsa464712

Artificial Intelligence-Based Collaborative Control Method for Police UAV Cluster and Its Application in Social Governance

Ganbin Xu[1,*]
[1] Police Command and Tactics College, Zhejiang Police College, Hangzhou, Zhejiang, 310000, China
Corresponding authors: (e-mail: xuganbin@126.com).

Abstract The rapid development of artificial intelligence and UAV technology is driving the application of police UAV clusters in the fields of social governance and public safety. The article optimizes the coherent formation control of police UAV clusters based on the artificial intelligence algorithm of particle swarm. Its dynamics model is optimized according to the flight characteristics of quadrotor UAVs, and the convergence speed is further improved by the particle swarm algorithm. Introducing rounded variables in the discrete-time control barrier function makes the UAV more natural in the obstacle avoidance process. The range of the Liapunov function is adaptively adjusted to improve the success rate of intersection construction. Meanwhile, the event triggering strategy is introduced to solve the optimal control variables for obstacle avoidance. The coherent formation control algorithm in this paper can complete the UAV converging to the reference trajectory along the X-axis and Y-axis within 0.5 seconds. The clustering success rate of the event-triggered obstacle avoidance strategy is improved by 5.84% to 18.95% compared with the comparison algorithm. The police UAV using the cooperative control method in this paper monitors that the PM2.5 concentration on urban roads is significantly reduced after water sprinkling. For a comprehensive evaluation result of water quality in a watershed is 0.139, which belongs to class II water quality. The UAV cluster can be linked with the city management system to build an all-round and three-dimensional governance system.

Index Terms Artificial Intelligence, Particle Swarm Algorithm, Lyapunov Function, Cooperative Control Algorithm, Police Drone

I. Introduction

In recent years, with the in-depth application of UAVs in counter-terrorism investigation [1], search and rescue [2], patrol and monitoring [3], explosion-proof search and arrest [4] and other work, it has become an important tool for public security organs to safeguard people's safety and maintain social stability in police work. First of all, police drones extend the policing space and can act in the airspace. It establishes the airspace as a new regulatory field and promotes the gradual penetration of police work into the air [5], [6]. Second, police drones shape the object of policing. The air domain is not only a space for police enforcement, but the elements in it become the objects of police enforcement, and the control of the air domain is strengthened in the interaction [7], [8]. Finally, police drones transform police operations and enable the instrumentalization of the aerial domain. The spatial and temporal logic of police drones changes their operational logic, and their aerial gaze provides a multidimensional and long-distance observation that can improve the accuracy and mobility of observation [9]-[11]. Their implementation and deployment can be localized to a specific time, which facilitates the observation and understanding of past and present events, and can also guide future actions [12].

However, at present, the application of UAVs in the policing work of public security organs is mostly limited to one-man operation, i.e., a police officer with flight qualification can only operate one UAV at the same time [13], [14]. Therefore, when multiple UAVs are needed to perform a certain task, a corresponding number of police officers are required to maneuver them. Police UAV clustering technology is a multi-drone cooperative technology, which can effectively integrate the hardware and software resources owned by multiple drones themselves, as well as the information collected and processed [15]. Compared with a single police UAV, police UAV cluster technology can utilize limited police force to manipulate multiple UAVs to complete police work such as investigation, search and arrest, patrol and monitoring, thus enhancing police effectiveness [16]-[18]. Therefore, the study of UAV cluster cooperative control methods based on artificial intelligence can effectively broaden the application scenarios of police UAVs and better apply to police combat [19], [20].

At present, the research on distributed cooperative control of UAV swarm system is getting more and more attention. For example, for its formation problem, Ouyang, Q. et al. described the complete formation control process

of UAV cluster from formation assignment to formation transition, and pointed out that distributed formation control strategy is an important method for UAV formation control based on comparative analysis [21]. Kada, B. et al. applied a distributed coherence algorithm to a multi-intelligent body system oriented to the cooperative control of multiple UAVs by providing them with smooth inputs and realizing 3D formation tracking of UAV formations by introducing a geometric pattern model [22]. Liu, L. et al. designed a distributed cooperative control method for UAV swarms that utilizes a formation error system to reconstruct and maintain the UAV cluster formation to achieve formation speed consistency [23]. Jiang, Z. H. A. O. et al. designed a cooperative control scheme for UAV clusters based on the role cost function based on distributed model predictive control, which achieves cooperative control of UAVs in ideal formation by optimizing the role of each UAV for each heterogeneous role [24]. Dey, S. and Xu, H. proposed hierarchical learning algorithms to learn optimal group control strategies for multi-group leaders and decentralized group control strategies for large-scale followers based on large-scale multi-intelligent body systems and cooperative game models to improve the performance of collaborative control of UAV clusters [25]. Zhang, J. et al. designed a cooperative control algorithm for UAVs supported by a distributed coherence approach, which can perform tasks such as formation maintenance and transformations when the communication topology is determined [26].

In terms of communication issues, Goel, S. showed that localization of each node of a UAV swarm is an important prerequisite for carrying out cooperative control, and proposed a distributed cooperative swarm localization system based on low-cost sensors to achieve high-precision localization with better network connectivity [27]. Gao, N. et al. investigated an optimization approach for the UAV cluster wireless coverage problem by modeling the UAV cluster network as an undirected random graph and constructing a game model to solve the distributed optimization subproblem of wireless coverage [28]. Zhang, H. et al. examined a cooperative control method for UAVs under unstable network communication, using an ant colony optimization algorithm to bring the pheromone matrices of each UAV to consistency, i.e., solving the collision problem between UAVs and improving the cooperative control efficiency [29]. Venturini, F. et al. proposed the use of distributed reinforcement learning methods to enhance the exploration range of swarm UAVs for unknown regions and to realize context-aware implicit cooperative control with the help of information exchange over communication channels [30]. Ling, H. et al. constructed a scalable UAV swarm cooperative perception simulation platform with good compatibility and the ability to accurately simulate flight motion dynamics and noisy communications to provide support for UAV swarm cooperative planning [31]. Liu, W. and Gao, Z. Improvement of swarm control algorithm by using virtual leader helps multiple UAVs to accurately track the virtual leader to realize collision-free movement, and at the same time, the concept of virtual communication circle is introduced to control the communication power and distance, which guarantees the stability and safety of the communication between multiple UAVs [32].

Police UAV is a supplementary police equipment to cope with violent emergencies, and it plays an important role in practical police applications, which not only has the demand of carrying light weapons such as tear gas, concussion and smoke, but also needs to realize precise strikes and tracking in tasks such as encircling and arresting criminals. Therefore, it is crucial to explore the cooperative control method applicable to police UAV clusters, which is conducive to promoting the informationization construction of public security organs.

In this study, the feedback linearization method is adopted to realize the control of UAV spatial position and Euler angle changes, so as to obtain its linearized dynamics model. Using the particle swarm optimization algorithm, the optimal speed of UAV flight is solved, and the constraints are incorporated to complete the coherent formation control of UAV cluster. For the UAV cluster obstacle avoidance problem, a distributed non-collaborative obstacle avoidance model is designed. The conflict resolution factor is introduced to improve the overall construction success rate by adaptively adjusting the boundary of the Lyapunov function. Event-triggered strategies are introduced into the predictive control phase of the model to generate new control sequences based on information feedback. Finally, the effectiveness of the UAV cluster cooperative control method proposed in this paper is demonstrated through simulation experiments and social governance applications.

II. Key technologies

II. A.Particle swarm based AI optimization algorithm

Particle Swarm Algorithm (PSO) [33] is a stochastic search optimization algorithm relying on group collaboration, which belongs to the category of computational intelligence in the field of Artificial Intelligence, and searches for the optimal path by simulating the mechanism of collaboration among flocks of birds.

The core of the particle swarm algorithm is to drive the whole swarm to gradually transform from disorder to order in the search space through information sharing and collaboration among individuals to seek the optimal solution. At the beginning of the algorithm, a swarm of particles is randomly generated and gradually approaches the optimal

solution through iterations. In each iteration, the particles update their velocities and positions using their own historical best position pbest and the global best position gbest of the population.

The particle velocity update formula is:

$$v_i = \omega \times v_i + c_1 \times r_1 \times (pbest_i - x_i) + c_2 \times r_2 \times (gbest_i - x_i) \tag{1}$$

where ω is the inertia factor, r_1, r_2 is the random number of (0, 1), x_i is the current position of the particle, v_i is the current velocity of the particle, and c_1, c_2 is the learning factor.

The particle position update formula is:

$$x_i = x_i + v_i \tag{2}$$

where x_i is the current position of the particle and v_i is the velocity of the particle.

The position update of each particle is obtained by adding the current position x_i and the velocity v_i of the next time step. This velocity vector affects the direction and speed of the particle's movement in the search space.

II. B.Liapunov Stability

In control systems, there are many factors that affect stability. If these influencing factors are not controlled, the original stable equilibrium state will be broken, causing incalculable harm. In 1892, the famous Russian mechanic Liyapunov first proposed the concept of motion stability [34], and put forward two methods of stability analysis: Liyapunov's first method and the second method.

Liapunov's first method, first linearizes the nonlinear system in a small neighborhood, and then determines the stability of the system by eigenvalue analysis, so it is also known as the small range stability analysis method. If there are positive real parts in the eigenvalues of this linear system, the system is unstable in this small neighborhood. If the eigenvalues of the system are all negative real parts, the system is satisfied with stability in the small neighborhood. If the eigenvalues include both negative and zero real parts, the stability of the system requires further analysis.

Liapunov's second method is a research method that determines whether a system is stable or not directly based on its structure. For a nonlinear system, the stability of the system is determined by introducing the Lyapunov function and then taking the derivative of the Lyapunov function along the structural equations of the system, based on the positive or negative of the derivative. If the derivative of the Liapunov function is negative, the system is stable. In terms of the energy properties of the physically meaningful Liapunov function, it means that the energy decreases over time and eventually reaches an equilibrium state.

III. Artificial intelligence-based cooperative control method for police unmanned aircraft clusters

In this section, particle swarm algorithm is mainly used to realize the research of optimization method on police UAV cluster cooperative control, to complete the autonomous cooperative operation of UAV cluster, and to carry out simulation to verify the effectiveness of the method in this paper.

III. A. Particle swarm optimization for optimal coherent formation control

III. A. 1) Feedback linearization model for quadcopter UAVs

When simplifying the quadrotor UAV dynamics model, it is usually assumed that the quadrotor UAV is more compact, the air has less drag effect on it during flight, and the rate of change of the angular rate and Euler angle are approximately equal at the near hovering point. Therefore there is:

$$\begin{cases} \ddot{x} = \dfrac{U_1}{m}(\cos\phi\sin\theta\cos\psi + \sin\phi\sin\psi) \\ \ddot{y} = \dfrac{U_1}{m}(\cos\phi\sin\theta\sin\psi - \sin\phi\cos\psi) \\ \ddot{z} = \dfrac{U_1}{m}\cos\theta\cos\phi - g \\ \ddot{\phi} = \dfrac{U_2}{I_x} \\ \ddot{\theta} = \dfrac{U_3}{I_y} \\ \ddot{\psi} = \dfrac{U_4}{I_z} \end{cases} \tag{3}$$

where $[x,y,z]$ is the spatial position of the UAV in the coordinate system G, $[\phi,\theta,\psi]$ is the attitude angle of the UAV, $[I_x,I_y,I_z]$ is the rotational inertia component of the UAV in the three directional axes in the coordinate system B, respectively. $[U_1,U_2,U_3,U_4]$ represents the forces provided by the four axes of the quadrotor UAV, respectively, wherein U_1 provides a driving force in the direction of the Z_{b1}-axis, U_2 provides a torque in the X_{b1}-direction, U_3 provides a torque in the Y_{b1}-direction, and U_4 provides a torque in the Z_{b1}-direction, to realize the control of the altitude and the attitude angle of the quadrotor UAV in the three directions.

After inputting the forces provided by the four rotor axes of the UAV, the changes of the spatial position and Euler angles of the UAV can be output, so as to obtain the spatial position and Euler angles of the UAV in the current state. In this paper, the model of the above equation is processed through the feedback linearization method, so that $\ddot{z}=0$, through equation (3), can be expressed as U_1:

$$U_1=\frac{mg}{\cos\theta\cos\phi} \tag{4}$$

Combining Eq. (3) the differential equation for the state of the system in the horizontal direction can be obtained as:

$$\begin{cases}\ddot{x}=g(\dfrac{cos\phi sin\theta cos\psi}{cos\phi cos\theta}+\dfrac{sin\phi sin\psi}{cos\phi cos\theta})=g(tan\theta cos\psi+tan\phi\dfrac{sin\psi}{cos\theta})\\ \ddot{y}=g(\dfrac{cos\phi sin\theta sin\psi}{cos\phi cos\theta}-\dfrac{sin\phi cos\psi}{cos\phi cos\theta})=g(tan\theta sin\psi-tan\phi\dfrac{cos\psi}{cos\theta})\end{cases} \tag{5}$$

Assuming that there is $\psi\in[-90°,90°],\theta\in[-90°,90°]$ in Eq. (5) and $\Theta=0$, the system reaches unanimity when its system state quantities satisfy the following constraints:

$$\begin{cases}\lim_{t\to\infty}\|x_i-x_j\|=R_x\\ \lim_{t\to\infty}\|y_i-y_j\|=R_y\\ \lim_{t\to\infty}\|z_i-z_j\|=R_z\\ \lim_{t\to\infty}\|\Theta_i\|=0\end{cases} \tag{6}$$

where $[x_i,y_i,z_i]$ is the positional coordinate of the i nd UAV in coordinate system G and $\Theta_i=[\phi_i,\theta_i,\psi_i]$ is the Euler angle of the i th UAV. Then there are $\sin\phi\to0$ when the condition of Eq. (6) is satisfied, and there are $\tan\psi\to0$ and $\tan\theta\to0$ in Eq. (5), so Eq. (5) can be simplified as:

$$\begin{cases}\ddot{x}\approx g\tan\theta\\ \ddot{y}\approx -g\tan\phi\end{cases} \tag{7}$$

Then the nonlinear model of Eq. (3) can be expressed as:

$$\begin{cases}\ddot{x}=g\theta\\ \ddot{y}=-g\phi\\ \ddot{z}=\dfrac{U_1}{m}\cos\theta\cos\phi-g\\ \ddot{\phi}=\dfrac{U_2}{I_x}\\ \ddot{\theta}=\dfrac{U_3}{I_y}\\ \ddot{\psi}=\dfrac{U_4}{I_z}\end{cases} \tag{8}$$

In Eq. (8), U_1 no longer controls the acceleration in the directions of x and y, so that the acceleration of x is only related to θ, and the acceleration of y is only related to ϕ. The associated variables in Eq. (8) are

inductively classified, and the linearized dynamics model of the quadrotor UAV can be obtained by the feedback linearization method as:

$$\begin{cases} \dot{x}^{(0)} = x^{(1)} \\ \dot{x}^{(1)} = x^{(2)} \\ \dot{x}^{(2)} = x^{(3)} \\ \dot{x}^{(3)} = U_3^{'} \end{cases} \tag{9}$$

$$\begin{cases} \dot{y}^{(0)} = y^{(1)} \\ \dot{y}^{(1)} = y^{(2)} \\ \dot{y}^{(2)} = y^{(3)} \\ \dot{y}^{(3)} = U_2^{'} \end{cases} \tag{10}$$

$$\begin{cases} \dot{z}^{(0)} = z^{(1)} \\ \dot{z}^{(1)} = U_1^{'} \end{cases} \tag{11}$$

$$\begin{cases} \dot{\psi}^{(0)} = \psi^{(1)} \\ \dot{\psi}^{(1)} = U_4^{'} \end{cases} \tag{12}$$

For the above linear model, there are:

$$\begin{cases} U_1^{'} = \dfrac{\cos\phi\cos\theta U_1}{m} - g \\ U_2^{'} = -\dfrac{gU_2}{I_x} \\ U_3^{'} = \dfrac{gU_3}{I_y} \\ U_4^{'} = \dfrac{U_4}{I_z} \end{cases} \tag{13}$$

where $\left[U_1^{'}, U_2^{'}, U_3^{'}, U_4^{'}\right]$ is the control output of the consistency algorithm and $\left[U_1, U_2, U_3, U_4\right]$ is the control output of the actual UAS.

III. A. 2) Optimal consistency algorithm design based on particle swarm optimization

In order to further improve the convergence speed of the UAV, this section combines the particle swarm optimization algorithm to optimize the speed of the UAV. Taking velocity and acceleration as parameters to solve the optimal velocity at the current moment, the update model of its velocity can be expressed as:

$$\begin{cases} a(t+\Delta t) = \omega_\alpha a(t) + c_1 r_1 (pv - v(t)) + c_2 r_2 (gv - v(t)) \\ v(t+\Delta t) = v(t) + a(t)\Delta t \end{cases} \tag{14}$$

where $v(\tau), a(\tau)$ represents the velocity and acceleration at the moment of τ respectively, ω_α is a non-negative number representing the inertia weight, c_1, c_2 represents the learning rate of the particles converging to the corresponding state, r_1, r_2 represents a random number from 0 to 1, and pv, gv represents the local optimal speed and global optimal speed respectively. The flow of particle swarm optimization algorithm is shown in Figure 1:

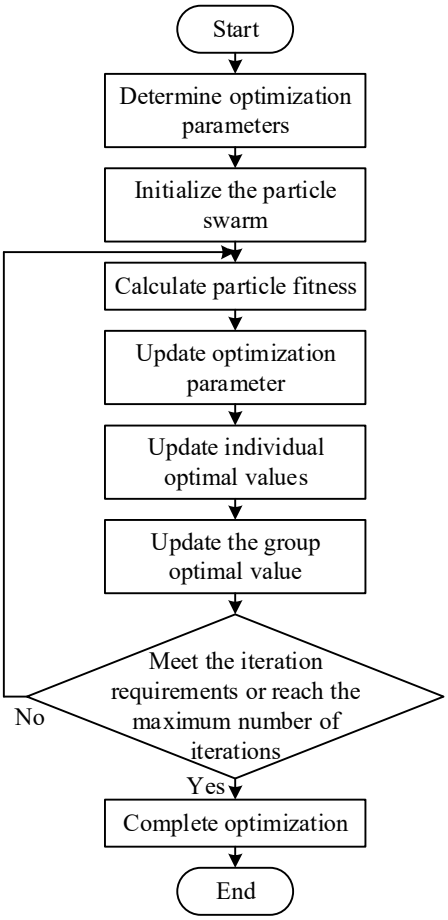

Figure 1: Flow chart of particle swarm optimization algorithm

In order to make the UAV realize the flight motion of the specified state, the amount of feedback state is increased, and the formation formation constraints, speed constraints, acceleration constraints of the UAV, and Euler angle constraints are added to make it more in line with the actual flight situation, and the improved algorithm can be expressed as follows:

$$\begin{cases} U_3^{'} = -m_i(\hat{X}_i - \hat{X}^*) - \sum_{j=1}^{N} a_{ij}\left[\gamma_0^Y(x_i - x_j - R_x) + \sum_{k=1}^{3}\gamma_k^Y(x_i^{(k)} - x_j^{(k)})\right] \\ U_2^{'} = -p_i(\hat{Y}_i - \hat{Y}^*) - \sum_{j=1}^{N} a_{ij}\left[\gamma_0^Y(y_i - y_j - R_y) + \sum_{k=1}^{3}\gamma_k^Y(y_i^{(k)} - y_j^{(k)})\right] \\ U_1^{'} = -q_i(z_i - \hat{Z}^*) - \sum_{j=1}^{N} a_{ij}\left[\gamma_0^Z(z_i - z_j - R_z) + \gamma_1^Z(\hat{z}_i - \hat{z}_j)\right] \\ U_4^{'} = -\sum_{j=1}^{N} a_{ij}\left[\gamma_0^Y(\psi_i - \psi_j) + \gamma_1^Y(\hat{\psi}_i - \hat{\psi}_j)\right] \end{cases} \tag{15}$$

where m_i, p_i, q_i is the control coefficient of X-direction velocity, Y-direction velocity, and Z-direction altitude, respectively, and $m_i, p_i, q_i > 0$, $\left[\dot{x}^*, \dot{y}^*\right]$ are the desired velocity of the UAV in the x, y-direction, z^* is the desired altitude of the UAV, and $[R^x, R^y, R^z]$ is the relative distance matrix of the UAV, respectively, which can be expressed as:

$$\begin{cases} R^x = \begin{bmatrix} x_{11} & x_{12} & \cdots & x_{1n} \\ x_{21} & x_{22} & \cdots & x_{2n} \\ \cdots & \cdots & \cdots & \cdots \\ x_{n1} & x_{n2} & \cdots & x_{nn} \end{bmatrix} \\ R^y = \begin{bmatrix} y_{11} & y_{12} & \cdots & y_{1n} \\ y_{21} & y_{22} & \cdots & y_{2n} \\ \cdots & \cdots & \cdots & \cdots \\ y_{n1} & y_{n2} & \cdots & y_{nn} \end{bmatrix} \\ R^z = \begin{bmatrix} z_{11} & z_{12} & \cdots & z_{1n} \\ z_{21} & z_{22} & \cdots & z_{2n} \\ \cdots & \cdots & \cdots & \cdots \\ z_{n1} & z_{n2} & \cdots & z_{nn} \end{bmatrix} \end{cases} \tag{16}$$

where $\left[x_{ij}, y_{ij}, z_{ij}\right]$ is the relative distance between the i nd UAV and the j rd UAV:

$$\begin{cases} x_i - x_j \to x_{ij} \\ y_i - y_j \to y_{ij} \\ z_i - z_j \to z_{ij} \end{cases} \tag{17}$$

Constraints are also added to the parameters such as velocity, acceleration and Euler angle of the UAV:

$$\begin{cases} v_{xi} \in [V_{x\min}, V_{x\max}], a_{xi} \in [a_{x\min}, a_{x\max}] \\ v_{yi} \in [V_{y\min}, V_{y\max}], a_{yi} \in [a_{y\min}, a_{y\max}] \\ v_{zj} \in [V_{z\min}, V_{z\max}], a_{zj} \in [a_{z\min}, a_{z\max}] \\ \phi_i \in [\phi_{\min}, \phi_{\max}] \\ \theta_i \in [\theta_{\min}, \theta_{\max}] \\ \psi_i \in [\psi_{\min}, \psi_{\max}] \end{cases} \tag{18}$$

At this point, the design of a coherent formation control algorithm for a cluster of quadrotor UAVs is completed.

III. A. 3) System stability analysis

In this section, the 4th order subsystem of the quadrotor UAV is analyzed for stability by means of the Liapunov method, which in conjunction with the designed consistency algorithm (15) can be expressed as:

$$\begin{cases} \dot{x}_i^{(0)} = x_i^{(1)} \\ \dot{x}_i^{(1)} = x_i^{(2)} \\ \dot{x}_i^{(2)} = x_i^{(3)} \\ \dot{x}_i^{(3)} = -m_i(x_i^{(1)} - v_x^* \otimes 1_n) - \gamma_0^x \left[Lx_i^{(0)} - diag(WR^x) \right] \\ -\gamma_1^x Lx_i^{(1)} - \gamma_2^x Lx_i^{(2)} - \gamma_3^x Lx_i^{(3)} \end{cases} \tag{19}$$

Then the matrix form of the system error equation of state of Eq. (19) can be expressed as:

$$\dot{\hat{X}}_i = \begin{bmatrix} 0_{n\times n} & I_n & 0_{n\times n} & 0_{n\times n} \\ 0_{n\times n} & 0_{n\times n} & I_n & 0_{n\times n} \\ 0_{n\times n} & 0_{n\times n} & 0_{n\times n} & I_n \\ -\gamma_0^x L & -\gamma_1^x L - m_i I_n & -\gamma_2^x L & -\gamma_3^x L \end{bmatrix} \hat{X}_i \tag{20}$$

where $\hat{X}_i$ is the 4-dimensional consistent system error state vector for a 4th order system, denoted as:

$$X_i = \left[\hat{x}_i^{(0)} \quad \hat{x}_i^{(1)} \quad \hat{x}_i^{(2)} \quad \hat{x}_i^{(3)} \right]^{\mathrm{T}} \tag{21}$$

where each systematic error is denoted as:

$$\begin{cases} \hat{x}_i^{(0)} = x_i^{(0)} - x_j^{(0)} - \Delta x_{ij} \\ \hat{x}_i^{(1)} = x_i^{(1)} - x_j^{(1)} - v_x^* \\ \hat{x}_i^{(2)} = x_i^{(2)} - x_j^{(2)} \\ \hat{x}_i^{(3)} = x_i^{(3)} - x_j^{(3)} \end{cases} \tag{22}$$

A non-singular transformation of the coefficient matrix in Eq. (20) yields the matrix P:

$$P = \begin{bmatrix} -I_n & I_n & 0_{n\times n} & 0_{n\times n} \\ -I_n & 0_{n\times n} & I_n & 0_{n\times n} \\ -I_n & 0_{n\times n} & 0_{n\times n} & I_n \\ P_{41} & P_{42} & P_{43} & P_{44} \end{bmatrix} \tag{23}$$

Among them:

$$\begin{aligned} P_{41} &= -\gamma_0^x L + \gamma_1^x L + m_i I_n - I_n \\ P_{42} &= -\gamma_1^x L - m_i I_n + \gamma_2^x L \\ P_{43} &= -\gamma_2^x L + \gamma_3^x L \\ P_{44} &= -\gamma_3^x L + I_n \end{aligned} \tag{24}$$

An elementary transformation of matrix P yields matrix P_e:

$$P_e = \begin{bmatrix} -I_n & 0_{n\times n} & 0_{n\times n} & 0_{n\times n} \\ 0_{n\times n} & -I_n & 0_{n\times n} & 0_{n\times n} \\ 0_{n\times n} & 0_{n\times n} & -I_n & 0_{n\times n} \\ 0_{n\times n} & 0_{n\times n} & 0_{n\times n} & -L \end{bmatrix} \tag{25}$$

Then the rank of matrix P_e is $rank(P_e) = 4n-1$. Its approximate standard type is:

$$P_J = \begin{bmatrix} w_1 & \cdots & w_{4n} \end{bmatrix} \begin{bmatrix} 0 & 0_{1\times(4n-1)} \\ 0_{(4n-1)\times 1} & J \end{bmatrix} \begin{bmatrix} v_1^{\mathrm{T}} & \cdots & v_1^{\mathrm{T}} \end{bmatrix}^{\mathrm{T}} \tag{26}$$

where w_i, v_i^T are the left and right eigenvectors corresponding to eigenvalue 0, respectively. J' is the corresponding block diagonal matrix in approximate form. It can be obtained:

$$E_J = \begin{bmatrix} w_1 & \cdots & w_{4n} \end{bmatrix} \begin{bmatrix} 0 & 0_{1\times(4n-1)} \\ 0_{(4n-1)\times 1} & e^{j'} \end{bmatrix} \begin{bmatrix} v_1^{T} & \cdots & v_1^{T} \end{bmatrix}^{T} \tag{27}$$

where all non-zero eigenvalues have non-positive real parts and hence $e^{f_t} \to 0_{(2n-1)\times(2n-1)}$. Therefore, the fourth-order subsystem of the quadrotor UAV is asymptotically stable.

The matrix form of the state equation of the second order subsystem (11) of the quadrotor UAV can be expressed as:

$$\begin{bmatrix} z_i^{(1)} \\ \dot{z}_i^{(1)} \end{bmatrix} = \begin{bmatrix} 0_{n\times n} & I_n \\ -\gamma_0^z L & -\gamma_1^z L \end{bmatrix} \begin{bmatrix} z_i \\ \dot{z}_i \end{bmatrix} \tag{28}$$

Define the Lyapunov function $V(z,t)$ as:

$$V(z,t) = \frac{1}{2} z^{(1)T} z^{(1)} + \frac{\gamma_0^z}{2} z^{(0)T} L z^{(0)} \tag{29}$$

The derivative of $V(z,t)$ with respect to time is:

$$\begin{aligned}\dot{V}(z,t) &= z^{(1)T}\dot{z}^{(1)} + \gamma_0^z z^{(0)T} L z^{(1)} \\ &= z^{(1)T}(-\gamma_0^z L z^{(0)} - \gamma_1^z L z^{(1)} + \gamma_0^z L z^{(0)}) \\ &= -\gamma_1^z z^{(1)T} L z^{(1)} \le 0\end{aligned} \tag{30}$$

Then $V(z,t) \ge 0, \dot{V}(z,t) \le 0$, the quadrotor second-order subsystem is obtained to be asymptotically stable at the origin equilibrium state.

III. A. 4) Simulation experiments

In order to verify the effectiveness of the algorithm in this section when acting UAV formation in a two-dimensional environment, the algorithm is numerically simulated in MATLAB software. In this section, the numerical simulation of the UAV formation control algorithm is performed with the initial conditions of the UAV as shown in Table 1.

Table 1: Initial conditions for drones

Number	Expectation Angle	Initial relative position(x,y)(m)
UAV1	0	(-70,10)
UAV2	Π/6	(-30,10)
UAV3	Π/9	(10,50)
UAV4	-π/6	(50,50)
UAV5	-π/9	(60,10)

In the simulation experiment, the simulation duration is 8s, the sampling time is 0.2s, and the prediction time domain is 7. The UAV speed is in [5, 10] m/s.

(1) Tracking trajectory under initial ideal state

The position tracking trajectories of the UAV along the X-axis direction and Y-axis direction are simulated under the initial ideal state as shown in Figure 2 and Figure 3, respectively. As shown in the figure, in the X-axis direction, the UAV rapidly approaches along the reference trajectory from the given initial position at 0 s. It rejoins the reference trajectory after about 0.3 s, and the difference in distance from the trajectory is about 10.5 m. The trajectory is then tracked in the X-axis direction and in the Y-axis direction. Similarly, all UAVs along the Y-axis direction converge from the initial position of the Y-week after 0.5 s, indicating that rapid stabilization is also achieved in the Y-direction. From the figure, it can be seen that the controller responds quickly and is able to adjust the state of the UAVs in a very short period of time with good overdynamic performance after a short period of time under the given ideal environment.

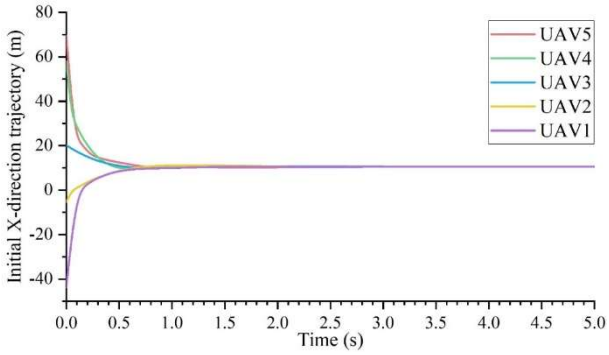

Figure 2: The drone tracks the location of the X-axis

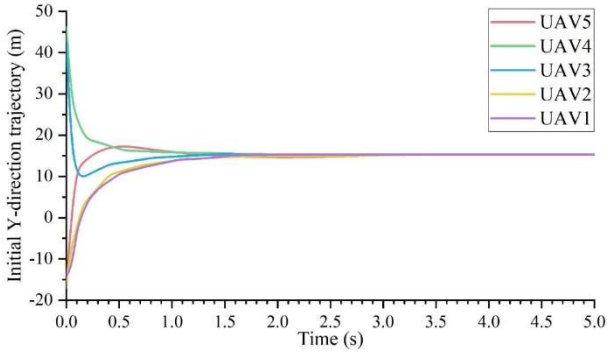

Figure 3: The drone tracks the location of the Y-axis

(2) Error curve when adding the perturbation signal as a time variable

Set the perturbation amount as F*sin(t), where F is the constant of stochastic simulation, and F=0.6 is taken here, and apply the same perturbation to the predictive controller of the model constructed in this paper, and the obtained UAV's following errors are shown as follows, and Figure 4, Figure 5, and Figure 6 are the UAV in the X-axis direction, the Y-axis direction, and the velocity error, respectively. From Figure 4, it can be seen that by applying the formation control method of this paper, the UAV's tracking error quickly converges to 0, indicating that the formation control method of this paper effectively suppresses the perturbation and improves the tracking accuracy. For the convergence of the error in the Y-axis direction, it can be seen from Figure 5 that the system's error in the Y-axis direction appears to converge faster after applying the control strategy of this paper. The method in this paper performs better against periodic perturbations, and its velocity error curve can be stabilized quickly after coping with the perturbations. This indicates that the algorithm in this paper has good robustness and can maintain system stability performance under external perturbations.

To summarize, the algorithm designed in this paper can counteract the effects of perturbations in a shorter time, thus maintaining the stability of the system.

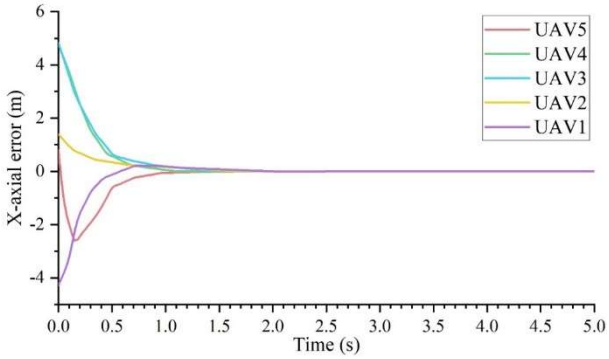

Figure 4: The error of the drone in the X-axis

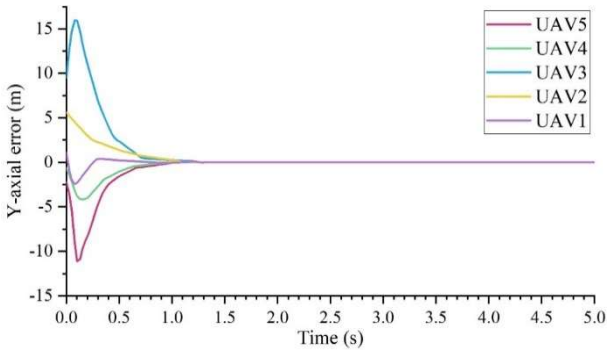

Figure 5: The error of the drone in the Y-axis

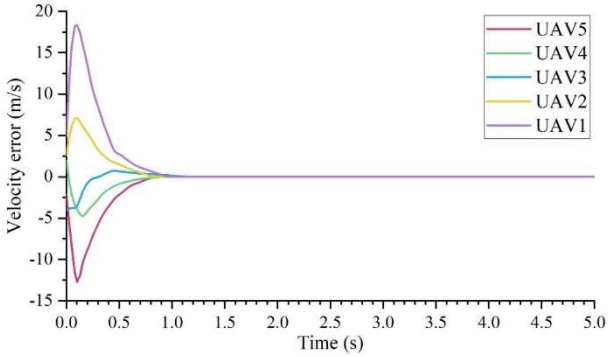

Figure 6: The velocity error of the drone

III. B. Obstacle avoidance controller design

The optimal performance release for UAV obstacle avoidance control problems is usually realized near the boundaries of state constraints and input constraints, and model predictive control has some execution advantages in related problems. In this section, a model predictive obstacle avoidance controller relying on event triggering is designed. This approach relies on the nonlinear model predictive control (MPC) framework [35], which unites Lyapunov functions (CLFs) and control barrier functions (CBFs) [36] for obstacle avoidance control. The overall control behavior is shown in Figure 7.

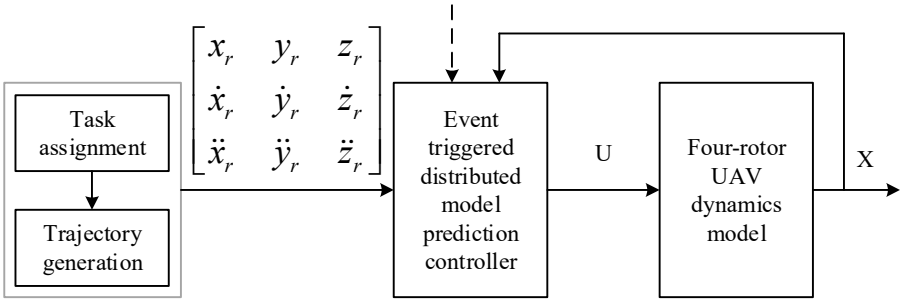

Figure 7: Overall control behavior

III. B. 1) Safety filter design

In this paper in order to emphasize that the constraint states satisfying the CBF constraints are safe and secure, the design process based on the control barrier function is externally represented as a secure filter construction, with the corresponding security and fastness depending on the expected level of satisfaction with the performance of the controlled object.

D-CBF is a subset of CBF over X, which is abstracted from standard CBF as a special case. In the theory of standard CBF, the security set C is positively invariant and asymptotically stable. Migrating the controlled object to the UAV application scenario can be obtained that the subset of C corresponding to the UAV position information also has positive invariance and asymptotic stability, which means that the whole control system is secure. The model of D-CBF is obtained:

$$\sup_{u\in U}\left[L_f h + L_g h u + \underbrace{\frac{\partial h}{\partial x_{obs}}\cdot\frac{\partial x_{obs}}{\partial t}}_{\varphi} + \underbrace{\frac{\partial h}{\partial \eta_{obs}}\cdot\frac{\partial \eta_{obs}}{\partial t}}_{\phi}\right] \geq -\gamma h \tag{31}$$

γ is a constant, and φ,ϕ is used to reflect the effect of changes in the position and shape of the obstacle on the input variables, respectively. The definition of the set of control variables is carried out here:

$$\begin{aligned} K_{D-CBF} &= \left\{u\in U : L_f h + L_g h u + \varphi + \phi \geq -\gamma h\right\} \\ K_{CBF} &= \left\{u\in U : L_f h + L_g h u \geq -\gamma h\right\} \end{aligned} \tag{32}$$

By mathematical reasoning, when $\varphi+\phi>0, K_{CBF} \subseteq K_{D-CBF}$. when $\varphi+\phi<0, K_{D-CBF} \subseteq K_{CBF}$. when $\varphi+\phi=0, K_{D-CBF}=K_{CBF}$.

For the discrete system, in order to make the trajectory of the whole UAV obstacle avoidance process more rounded, in this paper, the dynamic obstacles appear in the predicted safe area of the UAV in a certain observation time, for this reason, the rounded variable ω_h is introduced in the expression of D-CBF in discrete time, then:

$$h(x_{k+1})-\omega_h(1-\gamma)h(x_k)\geq 0, 0<\gamma\leq 1 \tag{33}$$

The form of D-CBF is obtained as follows:

$$h(x_k)=\| p_Q(k)-x_{obs}^i(k) \|_2 -l_i(k)-d_{safe}^{obs,i}-d_{safe}^{uav,Q} \tag{34}$$

$d_{safe}^{obs,i}$ is the safety expansion scale, and $d_{safe}^{uav,Q}$ is the minimum distance between UAV paddles without dynamics.

III. B. 2) Binding Conflict Dissolution

In this section, it is assumed that the allowable control input K_{adm} in the system can be described as a convex polygon with a fixed number of nodes, and the region in the input space that satisfies the CLF constraints is defined as $K_{CLF}=\{u\in U: L_fV+L_gVu\leq -\alpha V\}$. In order to increase the ability of the control strategy to abate the potential conflicts between the CLF and the D-CBF constraints, this paper adds a factor of unwrapping in the design of the CLF model, which can ensure the stability of the system by adjusting the range of the CLF adaptively and make the intersection more likely to be successfully constructed at the same time. At the same time, the possibility of successful construction of the intersection is increased, which leads to the derivation of $\Delta V(x_k,u_k)\leq -\alpha V(x_k)+\Theta_k, 0<\alpha\leq 1$. Accordingly, the ablation of conflicts at the constraint level is realized without affecting the stability of the system.

III. B. 3) Obstacle avoidance control model

Regarding the non-collaborative scenario obstacle avoidance problem, for System $x_{t+1}^i=f_i(x_t^i,u_t^i)$, the UAV cluster distributed non-collaborative obstacle avoidance model is:

$$\begin{aligned} &J_t^*(x_t)=*\min_{u_{t:t+N-1|t}} p(x_{t+N|t})+\sum_{k=0}^{N-1} q(x_k,u_k)+\zeta(\Theta_k) \\ &\begin{cases} x_{k+1}=f(x_k,u_k), k=0,..,N-1 \\ x_k\in X, u_k\in U, k=0,\ldots,N-1 \\ x_{t|t}=x_t \\ h(x_{k+1})-\omega_h(1-\gamma)h(x_k)\geq 0, \omega_h\geq 0, 0<\gamma\leq 1 \text{ for } k=0,\ldots,N-1 \\ V(x_{k+1})\leq (1-\alpha)V(x_k)+\Theta_k, 0<\alpha\leq 1 \text{ for } k=0,\ldots,N-1 \end{cases} \end{aligned} \tag{35}$$

The controller's prediction step $N=dt/\Delta T$, dt is the controller's prediction time domain, and ΔT is the sampling period.

$h(x_{k+1})-\omega_h(1-\gamma)h(x_k)$ denotes the safety filter implementation conditions for obstacle avoidance control, and the filter constraints are relaxed to a certain extent using the slack variable ω_h , considering that the brief appearance of dynamic obstacles or neighboring UAVs in the predicted safety zone during a certain observation time does not affect the safety in actual flight. $V(x_{k+1})$ The relevant conditional subformula describes the solution to the problem of potential conflicts between the CLF and dynamic CBF when used as a joint constraint by introducing a conflict resolution factor Θ_k , which improves the overall construction success rate by adaptively adjusting the boundaries of the CLF, $\zeta(\Theta_k)$ with the relaxation factor-related expression.

In the path tracking task, the stage cost function can be described as:

$$q(x_k,u_k)=a_x\| x_k-x_{plan} \|_2^2+a_u\| u_k \|_2^2+a_{\tilde{u}}\| u(1)-\tilde{u} \|_2^2+a_u\left\| \frac{u_k-u_{k-1}}{t_s} \right\|_2^2 \tag{36}$$

The first term describes the deviation of the UAV from the reference path, and $a_x > 0$ is the state quantity deviation coefficient. When the response amplitude of the UAV maneuver is large, it will cause greater energy consumption, so the second term is used to construct a tracking energy consumption index to constrain the amplitude including angular velocity and acceleration, and $a_u > 0$ is the control volume energy consumption coefficient. Since the presence of large fluctuations between successive control decisions may cause the controller to fail to respond in time to the incoming control commands, the third term is used to constrain the difference between the first component of the control volume and the initial control volume using the third term, $a_{\tilde{u}} > 0$ describes the response weighting coefficient. The last term then describes the rate of change of the control quantity.

III. B. 4) Event triggering mechanisms

In this paper, we introduce an event-triggered strategy into the predictive control phase of the model by introducing a cache to store the optimal control sequence of the current node. At each time step, the event monitor decides whether to fuse the sensed information to co-generate a new control sequence based on the information feedback from the PLANT, and if no event occurs, the next moment control input from the cache is deferred. Given a conditional paradigm for event triggering:

If $g_i(x_t, u_t) \geq 0, a_t = 1$, the control variable update is performed $u_{t_p} \leftarrow u^*_{t_p|t_p}$, $u^*_{t_p|t_p}$ is the optimal control variable for the NMPC problem solved at the moment of event triggering t_p.

The design of the main event triggering conditions in this paper is given below:

Condition 1: The predicted distance between the UAV and the obstacle is about to be less than the safe distance when there is no other strategy to interrupt the current controlled state, denoted as:

$$g_i(x_t, u_t) = \Delta d_i(t) = d_{safe} - d^{pred}_{uav} \tag{37}$$

d^{pred}_{uav} is the distance of the UAV from the obstacle under a certain predicted field of view.

Condition 2: describes the situation where there is a potential collision between the planned trajectories of the two UAVs in a non-collaborative relationship, given the non-collaborative scenario, the principal UAV i performs active and complete obstacle avoidance, disregarding the auxiliary adjusting behavior of the other UAV, to safeguard rapidity. Therefore it is denoted as:

$$g_i(x_t, u_t) = \Delta p_{ij}(t) = \| p^{pred}_i - p^{plan}_j \|_2 - d^{uav_{ij}}_{safe} \tag{38}$$

d^{uavij}_{safe} indicates $UAVi, j$ the minimum safe distance subject to kinematic and dynamic influences.

III. B. 5) Simulation experiments

In order to simulate various obstacles that may appear in real community environments and to verify the generalizability and feasibility of the obstacle avoidance algorithm in this paper, 100 simulation scenes were randomly generated. The number, location and size of various obstacles in each scene are randomized within a certain range, and 50 rounds of testing are conducted for each scene, with a total of 5000 rounds of testing. The average value obtained from 50 rounds of testing was taken for each simulation scene to compare the performance indexes, in order to exclude the chance results in testing and verify the performance evaluation indexes of the algorithm. Commonly used UAV cluster obstacle avoidance algorithms are selected for comparison with the algorithms in this paper, including Multi-Intelligent Two-Delay Depth Deterministic Strategy Gradient (MATD3) algorithm, Improved DDPG based on LSTM network (LSTM-DDPG) algorithm, Task Decomposition-based Multi-Intelligent Two-Delay Depth Deterministic Strategy Gradient (TD-MATD3) algorithm, and Multi-Intelligent Dynamic Obstacle Sharing Mechanism Long Short-Term Memory (DM-MATD3) algorithm. The specific test comparison results are as follows:

(1) Comparison test of algorithm clustering success rate in randomized scenarios

Cluster Success Rate (CSR): In the test scenario, this round of test is considered successful only if all the UAVs in the cluster have avoided all the obstacles within the limited number of steps and successfully reached the specified target location. The cluster success rate can be defined as:

$$CSR = \frac{K}{M} \tag{39}$$

Where K is the number of times the UAV cluster successfully reached the target location, and M is the total number of UAV cluster test flights. A higher cluster success rate indicates that the algorithm is more performant and more suitable for fixed-wing UAV cluster cooperative dynamic obstacle avoidance tasks.

In the tests in this subsection, the five algorithms are tested to perform the tasks under 100 generated random scenarios, and the cluster success rate of each scenario is calculated and counted as shown in Figure 8. From the figure, it can be seen that under 100 random scenes, the cluster success rate achieved by the UAV obstacle avoidance algorithm proposed in this paper is mainly distributed between 93%-97%, with a small range of fluctuations, and are all higher than the remaining four algorithms, with an average cluster success rate of 94.93%.The MD-MATD3 algorithm has a larger fluctuation range, and achieves a higher cluster success rate, with an average cluster success rate of 89.04%. The MATD3 algorithm cluster success rate is significantly lower than the remaining four algorithms, with an average cluster success rate of 75.98% respectively. Using this paper's algorithm to perform the quadrotor UAV cluster cooperative dynamic obstacle avoidance task in random scenarios, the average cluster success rate is improved by 5.84% to 18.95% compared to the comparison algorithms. The use of this paper's algorithm for quadrotor UAV clusters can effectively improve the cooperative dynamic obstacle avoidance ability of UAV clusters in random battlefield environments and enhance the cluster success rate.

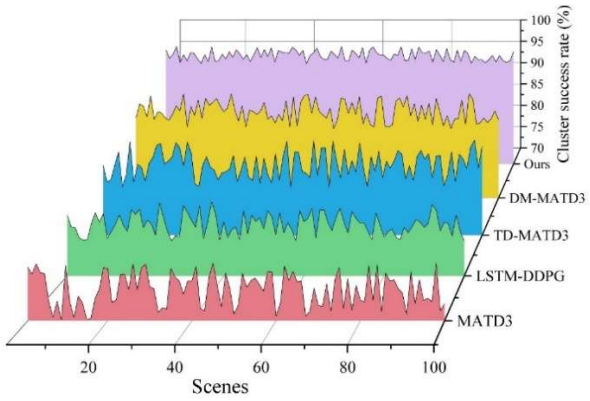

Figure 8: Cluster success rate of each scene

(2) Comparison test of algorithm cluster crash rate in random scenarios

Cluster Crash Rate (CCR): the cluster crash rate is also the main basis for evaluating the performance of the algorithm, as long as one UAV in the cluster crashes, the cluster is considered to have crashed. The crash rate can be defined as e.g:

$$\mathrm{CCR}=\frac{J}{M} \tag{40}$$

where J is the number of times the UAV cluster successfully reaches the target location, and M is the total number of UAV cluster test flights. The lower crash rate indicates that the algorithm is more performant and more suitable for fixed-wing UAV cluster cooperative dynamic obstacle avoidance tasks.

In the tests in this subsection, the five algorithms are tested to perform the task under 100 generated random scenarios, and the cluster crash rate of each scenario is calculated and counted as shown in Figure 9. As can be seen from the figure, under 100 random scenes, the cluster crash rate achieved by the algorithm proposed in this paper has a small range of fluctuation around 1%~5% and is lower than the remaining four comparison algorithms, with an average cluster crash rate of 3.12%; the MD-MATD3 algorithm achieves a relatively large fluctuation in the cluster crash rate, but the overall cluster crash rate is lower, with an average cluster crash rate of 7.43%; The MATD3 algorithm has slightly the highest cluster crash rate, with an average cluster crash rate of 26.49%. Using this paper's algorithm to perform the quadrotor UAV cluster cooperative dynamic obstacle avoidance task in random scenarios, the average cluster crash rate is reduced by 4.31% to 23.37% compared with the comparison algorithm. The use of this paper's algorithm for quadrotor UAV clusters can effectively improve the cooperative and obstacle avoidance capabilities of UAV clusters in random battlefield environments and reduce the cluster crash rate.

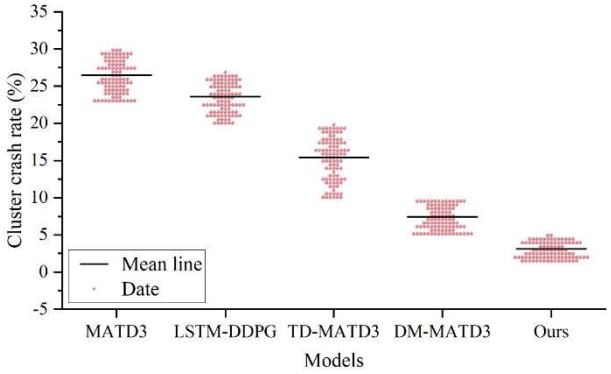

Figure 9: Cluster crash rates in each scene

IV. Application of police drones in social governance

In this section, the UAV equipped with the cluster cooperative control algorithm designed in this paper is applied to the air quality as well as water quality monitoring tasks in the community, and the value of the UAV under the algorithm of this paper is objectively evaluated for its application in social governance.

IV. A. Dynamic monitoring of dust suppression on urban roads

With many atmospheric pollutants such as dust, motor vehicle exhaust and various unfavorable factors, the task of combating air pollution is very serious, and urban air pollution has become one of the regional environmental problems. Through this paper, the designed cooperative control UAV carrying a sensor with measurement of PM2.5 at a height of 20m for measurement, so as to effectively evaluate the performance of the UAV in the dynamic monitoring of urban dust suppression.

Measuring the concentration of PM2.5 in the urban road before and after sprinkler sprinkling, the experimental analysis was carried out with the size of 200m×300m range area and the vertical height of 20m, and the monitoring results of PM2.5 concentration in the urban road before and after sprinkling were obtained, as shown in Figure 10 and Figure 11, respectively. Combining the results of the two figures, it can be seen that in the same area with a height of 20m, the PM2.5 concentration in the area of 200m×300m range before watering is 44μg/m³~50μg/m³, while the PM2.5 concentration returned by the drone after watering is 33μg/m³~40μg/m³. The PM2.5 concentration after watering obtained by the drone is much lower than that before watering, and the PM2.5 concentration in urban roads before and after watering are as shown in Figs. 10 and 11 respectively. The decrease of PM2.5 concentration is especially obvious and the magnitude of the decrease is large. It shows that relying on UAV-carried sensors can be in different spatial and temporal environments of the air data samples, can make an effective evaluation of the dynamic changes of the limited spatial range of the short-effect time. The UAV cluster cooperative control method proposed in this paper can scientifically and intelligently control UAVs precisely and provide more technical support for air monitoring.

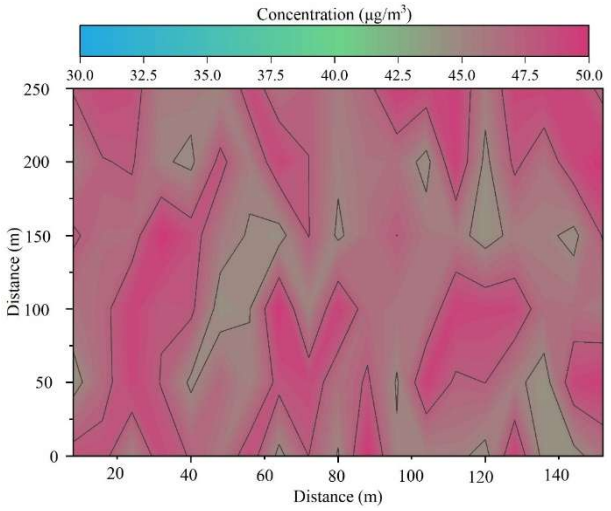

Figure 10: The concentration of the 20 m in the water is changed

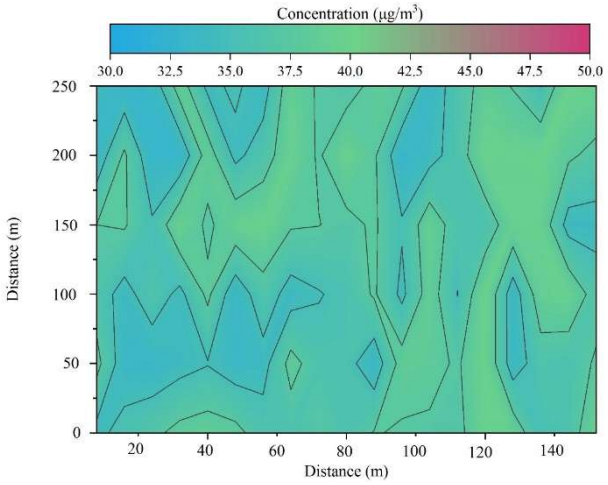

Figure 11: Changes in concentration of 20 m after sprinkling water

IV. B. Community watershed water quality monitoring

Intelligent manufacturing opened the curtain of the fourth industrial revolution, the drone as one of the products, its simple to use, easy to manipulate the characteristics of a number of current police work, especially in the water police scene disposal, in line with the needs of combat applications.

A watershed water quality fuzzy comprehensive evaluation system data based on river water quality parameters, including acidity and alkalinity (pH), chemical oxygen demand (COD), total phosphorus content (TP), ammonia and nitrogen content (NH3-N) and dissolved oxygen (DO). The water quality evaluation indexes were based on the average values of abundant water period, flat water period, dry water period and the whole year, and the target layer and criterion layer of the fuzzy comprehensive evaluation were constructed. Before establishing the judgment matrix for the target layer, the parameter priority is first determined, i.e., the importance between the parameters is compared. For the target layer, the annual average value of the water quality indexes has a higher priority than the average value of the water quality in the abundant water period, the average value of the water quality in the flat water period and the average value of the water quality in the dry water period. The period with the smallest flow was selected as the higher priority among the abundant, flat, and dry water periods because the smaller the amount of water the more obvious the effect of pollutants on water quality.

This paper uses the police drone described above to stratify the water quality indicators of 20 water quality sampling points in an urban watershed, and the calculation method is as described in the water quality evaluation model above, and after the calculation, the average value of the comprehensive water quality evaluation index is obtained as shown in Table 2. From the table, it can be seen that the contents of pH, COD, NH3-N, and DO in a watershed reached normal levels throughout the year, in the period of abundant water, in the period of flat water, and in the period of dry water. Whereas, TP was greater than 0.1 mg/L during the abundant and flat water periods, indicating that the total amount of phosphorus compounds in the water body is high, which may lead to eutrophication. However, the TP content reached normal levels throughout the year and during the dry water period.

Table 2: Statistical table of water quality index (unit: mg/L)

	pH	COD	TP	NH3-N	DO
Annual mean	7.092	0.091	0.071	0.161	6.458
Flood mean	7.089	0.094	0.167	0.123	6.679
Mean of flat water	7.065	0.09	0.0156	0.064	6.227
Mean of dry water	7.092	0.091	0.071	0.161	6.458
Normal range	6.5~8.5	<15	<0.1	<0.5	>5

The weights of pH, CODcr, TP, NH3-N, and DO under the yearly, abundant, flat, and dry periods are calculated using the method described above by calling Matlab Data Toolbox as shown in Figure 12. From the figure, it can be seen that in the evaluation of the various water quality indicators, the weight value occupied by the average value of the whole year is relatively larger than that of the abundant water period, flat water period and dry water period. Taking dissolved oxygen (DO) as an example, the weight values of the indicators under the whole year, abundant water period, flat water period and dry water period are 0.726, 0.091, 0.086, 0.097, respectively, which indicates

that this paper focuses more on the whole year situation of a certain watershed when monitoring the water quality of the watershed by using UAV.

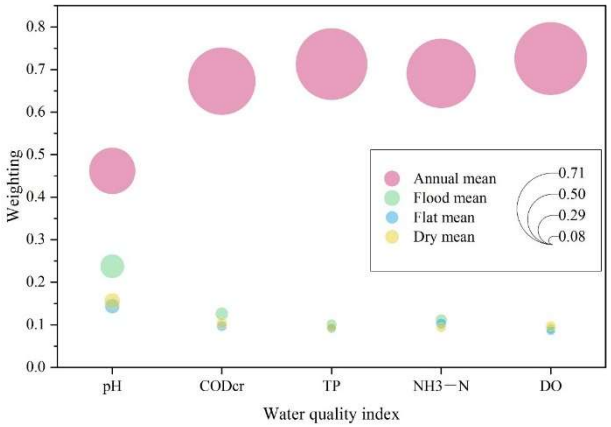

Figure 12: Weight of water quality evaluation index

Using Matlab data toolbox to calculate a comprehensive evaluation of water quality standards: $PI=\sum_{j=1}^{4}\sum_{i=1}^{5}(V_{Ai}\square V_{Bi}^{(i)})\beta_{ij}$ = 0.139. According to the comprehensive evaluation of water quality standards PI value of 0.10 ~ 0.25, is a class II water quality, that is, the overall water quality of a watershed to meet the standards, water quality is good.

Through the above method can get a watershed 20 sampling point water quality data, so as to find the fuzzy comprehensive evaluation index value, the use of the method described in this paper calculated by the final water quality of a watershed in various areas of the comprehensive evaluation of the results shown in Figure 13. As can be seen from the figure, the overall water quality of the investigated watershed is good and meets the standard of surface water quality class II, but there is mild pollution in observation point No. 6 and observation point No. 12 of a watershed. In order to further demonstrate the accuracy of the UAVs used in this paper, and to identify water quality problems in a watershed in a targeted manner, the project members went to observation points 6 and 12 in a watershed to carry out on-site investigations. According to the results of the field survey, the water quality of a watershed #6 exceeded the total phosphorus standard. Mainly due to its upstream side of the existence of a fertilizer plant, the plant has been shut down and relocated, but due to the raw material piles in the field has not been completed removal, resulting in rainfall wash part of the pollutants into the river, which caused the total phosphorus exceeded the water quality deterioration of the river in the region. 12 observation point area for the county is located in the region, the region has a relatively high density of population, and some of the riverside area of the existence of sewage discharge phenomenon, the phenomenon of riverside commercial encroachment on the river, resulting in the deterioration of the water quality of the river. Phenomenon, resulting in the deterioration of river water quality. According to the field investigation and experimental analysis results, it can be concluded that the results of UAV in water quality monitoring and evaluation are in line with the actual situation, and the degree of reliability is good.

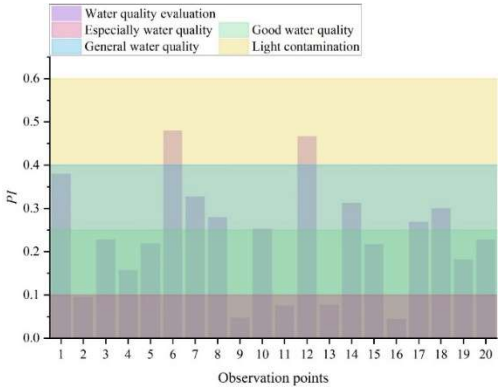

Figure 13: The results of water quality in various areas of a certain river basin

V. Conclusion

This paper explores the cooperative control method of police UAVs based on artificial intelligence and deeply analyzes the feasibility and advantages of its application in social governance. The dynamics model of the quadrotor UAV is simplified by a feedback sexualization model. Using the particle swarm optimization algorithm to solve the optimal speed of the UAV with speed and acceleration as parameters, the UAV formation control method is designed by combining the feedback state quantities and constraints such as formation formation and UAV speed. In addition, the UAV cluster obstacle avoidance control problem is solved with the help of event-triggered strategy. The UAV safety filter is constructed by controlling the barrier function, and the unblocking factor is added to the Lyapunov function to ensure the stable operation of the system.

The simulation experiment results show that:

(1) The coherent formation control method in this paper can maintain the stability of police UAVs in X-axis and Y-axis movement as well as speed under external disturbances, and the tracking error can be converged to 0 quickly.

(2) The success rate of police UAV clustering with event-triggered mechanism is improved by 5.84%~18.95% compared with the comparison method, and the corresponding crash rate is reduced by 4.31%~23.37%.

The social governance application experiments show that:

(1) The application of police UAVs with dynamic monitoring of urban road dust suppression can provide scientific and accurate data support for community air governance.

(2) Police UAVs in watershed water quality monitoring accurately predicted that the water quality evaluation standard PI of observation point 6 and observation point 12 exceeds 0.4, which is a mild pollution situation.

This paper proposes a complete set of police UAV cluster cooperative control method based on artificial intelligence, and simulates and field tests its effectiveness, which plays an obvious role in promoting social governance applications.

Funding

This work was supported by the National Social Science Fund of China for the project: "Research on the Legalization of Smart Policing" (Grant No. 23BFX127, 2023); and the Zhejiang Provincial Department of Education General Research Project for the project: "Research on the Impact Mechanism of Smart Policing on the Coordinated Development of Island Ecology and Economy - A Case Study of Zhoushan City" (Grant No. Y202455901, 2024).

References

[1] Gambo, A., & Ibrahim, M. O. (2022). Modelling and analysis of counter-terrorism: via drone. Mathematics and Computational Sciences, 3(3), 57-75.

[2] Van Tilburg, C. (2017). First report of using portable unmanned aircraft systems (drones) for search and rescue. Wilderness & environmental medicine, 28(2), 116-118.

[3] Gohari, A., Ahmad, A. B., Rahim, R. B. A., Supa'at, A. S. M., Abd Razak, S., & Gismalla, M. S. M. (2022). Involvement of surveillance drones in smart cities: A systematic review. IEEE Access, 10, 56611-56628.

[4] Choi, H., & Joung, K. W. (2024). A Study on the establishment of counter-drone system and the concept of integrated multi-domain defense. International Journal of Advanced Culture Technology, 12(4), 323-334.

[5] Saulnier, A., & Thompson, S. N. (2016). Police UAV use: Institutional realities and public perceptions. Policing: An International Journal of Police Strategies & Management, 39(4), 680-693.

[6] Yang, J., Ding, Z., & Wang, L. (2021). The programming model of air-ground cooperative patrol between multi-UAV and police car. IEEE Access, 9, 134503-134517.

[7] Yefimenko, I. M. (2022). Modern possibilities of using unmanned aerial vehicles by Police authorities and units: Analysis of foreign and Ukrainian experience. Scientific Journal of the National Academy of Internal Affairs, 27(3), 65-77.

[8] Beg, A., Qureshi, A. R., Sheltami, T., & Yasar, A. (2021). UAV-enabled intelligent traffic policing and emergency response handling system for the smart city. Personal and ubiquitous computing, 25(1), 33-50.

[9] Gokulakkrishnana, G., Nagendra Prasad, R., & Nijandan, S. (2015). Multifunctional Uav to Assist Police. International Journal of Engineering Research & Technology (IJERT), 4(2), 663-670.

[10] Heen, M. S., Lieberman, J. D., & Miethe, T. D. (2018). The thin blue line meets the big blue sky: Perceptions of police legitimacy and public attitudes towards aerial drones. Criminal Justice Studies, 31(1), 18-37.

[11] Georgiou, A., Masters, P., Johnson, S., & Feetham, L. (2022). UAV‐assisted real‐time evidence detection in outdoor crime scene investigations. Journal of forensic sciences, 67(3), 1221-1232.

[12] Qiu, Z., Liang, G., Du, H., Yan, B., Peng, J., & Ju, Z. (2023, November). A Police UAV System Based on Target Recognition. In International Conference on Computer Engineering and Networks (pp. 378-387). Singapore: Springer Nature Singapore.

[13] Chen, H., Gao, X., Li, H., & Yang, Z. (2024). A framework for the optimal deployment of police drones based on street-level crime risk. Applied Geography, 162, 103178.

[14] Engberts, B., & Gillissen, E. (2016). Policing from above: drone use by the police. The future of drone use: Opportunities and threats from ethical and legal perspectives, 93-113.

[15] Lorek, M., & Magniszewski, M. (2021). THE USE OF UNMANNED AERIAL VEHICLES BY THE POLISH POLICE. Journal of Security & Sustainability Issues, 11(1).

[16] Li, J., Xia, Y., & Cheng, Y. (2022, September). Application of UAV Remote Sensing Technology based on GIS in the Execution of Tasks of the People's Armed Police. In 2022 8th Annual International Conference on Network and Information Systems for Computers (ICNISC) (pp. 36-40). IEEE.
[17] Yuan-wu, S. H. I., & Xiao-cheng, Z. H. E. N. G. (2019). Application research on GQFD-TRIZ integration method in police UAV design. Journal of Graphics, 40(2), 296.
[18] Anania, E. C., Rice, S., Pierce, M., Winter, S. R., Capps, J., Walters, N. W., & Milner, M. N. (2019). Public support for police drone missions depends on political affiliation and neighborhood demographics. Technology in Society, 57, 95-103.
[19] Zhang, Z. (2022). Deconstruction of the application of police drone technology integrating Fourier fast transform algorithm in the 5G network era. Mathematical Problems in Engineering, 2022(1), 7718400.
[20] Miyano, K., Shinkuma, R., Shiode, N., Shiode, S., Sato, T., & Oki, E. (2020). Multi-UAV allocation framework for predictive crime deterrence and data acquisition. Internet of Things, 11, 100205.
[21] Ouyang, Q., Wu, Z., Cong, Y., & Wang, Z. (2023). Formation control of unmanned aerial vehicle swarms: A comprehensive review. Asian Journal of Control, 25(1), 570-593.
[22] Kada, B., Khalid, M., & Shaikh, M. S. (2020). Distributed cooperative control of autonomous multi-agent UAV systems using smooth control. Journal of Systems Engineering and Electronics, 31(6), 1297-1307.
[23] Liu, L., Liang, X., Zhu, C., & He, L. (2017, December). Distributed cooperative control for UAV swarm formation reconfiguration based on consensus theory. In 2017 2nd International Conference on Robotics and Automation Engineering (ICRAE) (pp. 264-268). IEEE.
[24] Jiang, Z. H. A. O., Jiaming, S. U. N., Zhihao, C. A. I., Yingxun, W. A. N. G., & Kun, W. U. (2022). Distributed coordinated control scheme of UAV swarm based on heterogeneous roles. Chinese Journal of Aeronautics, 35(1), 81-97.
[25] Dey, S., & Xu, H. (2022). Intelligent distributed swarm control for large-scale multi-uav systems: A hierarchical learning approach. Electronics, 12(1), 89.
[26] Zhang, J., Wang, W., Zhang, Z., Luo, K., & Liu, J. (2019, July). Cooperative control of UAV cluster formation based on distributed consensus. In 2019 IEEE 15th International Conference on Control and Automation (ICCA) (pp. 788-793). IEEE.
[27] Goel, S. (2017, September). A distributed cooperative uav swarm localization system: Development and analysis. In Proceedings of the 30th International Technical Meeting of The Satellite Division of the Institute of Navigation (ION GNSS+ 2017) (pp. 2501-2518).
[28] Gao, N., Liang, L., Cai, D., Li, X., & Jin, S. (2022). Coverage control for UAV swarm communication networks: A distributed learning approach. IEEE Internet of Things Journal, 9(20), 19854-19867.
[29] Zhang, H., Ma, H., Mersha, B. W., Zhang, X., & Jin, Y. (2023). Distributed cooperative search method for multi-UAV with unstable communications. Applied Soft Computing, 148, 110592.
[30] Venturini, F., Mason, F., Pase, F., Chiariotti, F., Testolin, A., Zanella, A., & Zorzi, M. (2021). Distributed reinforcement learning for flexible and efficient UAV swarm control. IEEE Transactions on Cognitive Communications and Networking, 7(3), 955-969.
[31] Ling, H., Luo, H., Chen, H., Bai, L., Zhu, T., & Wang, Y. (2021). Modelling and simulation of distributed UAV swarm cooperative planning and perception. International Journal of Aerospace Engineering, 2021(1), 9977262.
[32] Liu, W., & Gao, Z. (2020). A distributed flocking control strategy for UAV groups. Computer Communications, 153, 95-101.
[33] R. Parkavi,P. Karthikeyan & A. Sheik Abdullah. (2024). Enhancing personalized learning with explainable AI: A chaotic particle swarm optimization based decision support system. Applied Soft Computing,156,111451-.
[34] Reshma Ramaswami,Vinodkumar Arumugam & Sriramakrishnan Pathmanaban. (2025). Lyapunov conditions for the finite-time stability of fractional order disturbed nonlinear systems and neural networks: The secure image communication using encryption. Communications in Nonlinear Science and Numerical Simulation,145,108716-108716.
[35] Luca Caiaffa,Fabio Maran,Matteo Furlan,Stivi Peron,Alessandro Beghi & Mattia Bruschetta. (2025). Anti-wheelie systems for high-performance motorcycles: A Nonlinear Model Predictive Control approach. Control Engineering Practice,157,106224-106224.
[36] Liqun Ma,Yangchen Ding & Jianzhong Yang. (2025). Autonomous Emergency Gliding Landing Guidance and Control of Tilt-Wing Electric Vertical Take-Off and Landing for Urban Air Mobility Missions Using Control Barrier Functions. Aerospace,12(1),63-63.